Single-photon-level optical storage in a solid-state spin-wave memory

N. Timoney, I. Usmani, P. Jobez, M. Afzelius,[*] and N. Gisin

Group of Applied Physics, University of Geneva, CH-1211 Geneva 4, Switzerland

(Received 29 January 2013; published 20 August 2013)

A long-lived quantum memory is a firm requirement for implementing a quantum repeater scheme. Recent progress in solid-state rare-earth-ion-doped systems justifies their status as very strong candidates for such systems. Nonetheless an optical memory based on spin-wave storage at the single-photon level has not been shown in such a system to date, which is crucial for achieving the long storage times required for quantum repeaters. In this paper we show that it is possible to execute a complete atomic frequency comb (AFC) scheme, including spin-wave storage, with weak coherent pulses of $\bar{n} = 2.5 \pm 0.6$ photons per pulse. We discuss in detail the experimental steps required to obtain this result and demonstrate the coherence of a stored time-bin pulse. We show a noise level of $(7.1 \pm 2.3) \times 10^{-3}$ photons per mode during storage, and this relatively low noise level paves the way for future quantum optics experiments using spin waves in rare-earth-doped crystals.

PACS number(s): 03.67.Hk, 42.50.Ex, 42.50.Md

I. INTRODUCTION

Quantum communication, if rigorously executed, provides us with a provably secure method of communication [1]. However, inherently lossy channels limit the distance over which the communication can be performed, which today is roughly 250 km [2–4]. A quantum repeater can in principle allow quantum communication over longer distances [5–7], provided that the required quantum memories are developed. Prime candidates for quantum memories are atomic systems, which are capable of maintaining the coherence of stored excitations for long times. Atomic systems that are currently investigated range from individual quantum systems [8,9], laser-cooled atomic gases [10,11], and room-temperature atomic vapors [12–14] to rare-earth-ion-doped crystals [15,16]. In Ref. [7] a recent review can be found which compares different repeater and memory protocols used in these atomic systems. A more general review of quantum memories and their applications can be found in Ref. [17].

Crystals doped with rare-earth-ion impurities have attractive coherence properties when cooled below 4 K; in particular, hyperfine states can have coherence times which can approach seconds [18]. This has provided a strong motivation for developing quantum memories using such systems. Following the first storage experiment at the single-photon level [19], a succession of experiments demonstrated storage of single photons [20,21] and generation of light-matter [15,16] and matter-matter entanglement using crystals [22]. The quantum memory performances have also been strongly developed, particularly in terms of storage efficiency [23,24], multimode capacity [25,26], and polarization qubit storage [21,27,28].

These experiments were performed for short storage times (in the 10 ns to few μs regime) using an optical coherence, rather than exploiting long spin coherence times. Spin storage experiments require strong optical control fields to convert the initial optical coherence to a spin coherence. Photon noise is induced by such an operation, which has been nonetheless shown to work for alkali atomic systems [8–11,13,14].

In rare-earth-ion-doped solids the task is complicated since there is less spectral separation between the weak signal field and the optical control field (roughly 100 times less). Scattering from the control field is thus more likely as it propagates through a dense solid-state crystal.

Two quantum memory schemes were specifically proposed for solid-state ensembles; the controlled and reversible inhomogeneous broadening (CRIB) memory (see Ref. [29] and references therein) and the atomic frequency comb (AFC) memory [30]. The AFC has a particularly high multimode capacity, which is the ability to store trains of single-photon pulses [30,31]. This is crucial for speeding up quantum repeater protocols [6].

The AFC scheme is based on an echo induced by a regular spectral grating of periodicity Δ, in the absorption profile of an inhomogeneously broadened sample. The pulse to be stored in the memory is absorbed as a single excitation delocalized over the entire ensemble. The periodic spectral grating means that the affected atoms will rephase a time $1/\Delta$ after the initial storage and emit an echo (an AFC echo). The AFC echo is only a delay line, unless combined with spin-wave storage to achieve on-demand recall [30]. By this technique the optical coherence is transferred (written) to a spin coherence before the time $1/\Delta$ has elapsed. This operation is performed with a "control" pulse, essentially a π pulse over a particular bandwidth. This action stops the phase evolution of the spectral grating. Reversing the transfer, by applying the same control pulse again, restarts the phase evolution and retrieves an optical pulse as before (referred to as an AFC spin-wave echo). In addition to on-demand recall, this scheme allows for longer storage times due to longer spin coherence times. Yet, only a few AFC spin-wave storage experiments have been reported, all involving storage of bright classical pulses [32–34].

Here we demonstrate storage of an optical pulse containing a few photons on average, using an AFC memory combined with spin-wave storage in a europium-doped Y_2SiO_5 crystal. We apply a strategy of filtering in space, time, and frequency in order to reduce unwanted emission from the crystal at the moment the weak pulse is recovered from the crystal. To quantify the degree of noise, we measure the unconditional noise floor [13], which is the probability for the memory

————————
[*]mikael.afzelius@unige.ch

to produce a noise photon when the memory is read. We report that the unconditional noise floor can be reduced to $(7.1 \pm 2.3) \times 10^{-3}$ by our filtering strategy, which is low enough to allow for a range of quantum information schemes that require manipulation of spin coherence. Using the ability of the AFC memory to store multiple time bins, we also store and analyze a time-bin pulse with higher photon numbers, showing the high coherence of our memory.

This paper is organized as follows. We first describe our experimental setup (Sec. II) and preliminary memory properties in which bright optical pulses were stored (Sec. III). The main result of our paper, storage of weak coherent pulses, is shown in Sec. IV and coherence of the memory is shown in Sec. V. Finally we discuss our results and conclude the paper in Sec. VI.

II. EXPERIMENT SETUP

The crystal memory is europium-doped Y_2SiO_5 crystal. Europium is a promising candidate for quantum memories due to its fine coherence properties at T below 6 K [35–37], which ultimately could lead to an extremely long-lived [38] and multimode memory [30]. In this work we use the optical $^7F_0 \rightarrow {}^5D_0$ transition at 580 nm. The crystal is isotopically pure $^{151}Eu^{3+}$:Y_2SiO_5 (100 ppm). At a temperature of around 3 K we measure an overall absorption coefficient of $\alpha = 1.5$ cm^{-1} and an optical inhomogeneous linewidth of 500 MHz. The relevant energy diagram is shown in Fig. 1(a). Our input and control fields excite two optical-hyperfine transitions separated by 35.4 MHz.

The schematic of the experimental setup [Fig. 1(b)] shows only the optics around the cryostat containing the $^{151}Eu^{3+}$:Y_2SiO_5 crystal of length $L = 1$ cm. To reduce noise, the strong laser beam used for optical pumping and for the control pulses (control and preparation mode) is sent through
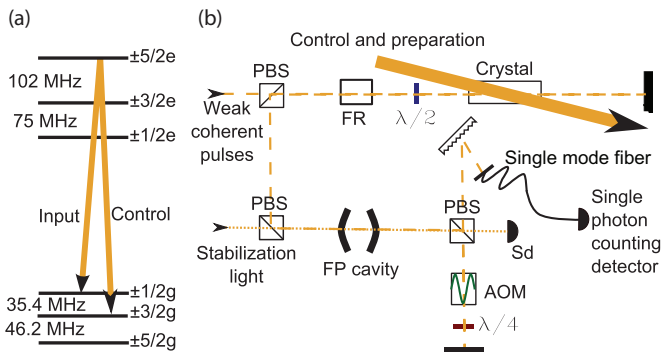
the crystal with a small angle with respect to the pulse to be stored and recalled (input mode). We estimate a spatial mode overlap of 95%. The laser and the AOMs used for spectral control are not shown in Fig. 1(b). The laser at 580 nm is a commercially available system based on an amplified diode laser at 1160 nm and a frequency-doubling stage. Before the cryostat the intense control pulses had peak powers of up to 300 mW. The diode laser is stabilized to have a spectral linewidth of approximately 30 kHz.

The AFC comb structures are created with frequency-selective optical pumping techniques [32,39]. The maximum optical depth we can achieve on the input transition is $\alpha L = 2.4$, in double-pass configuration.

III. BRIGHT PULSE STORAGE

We first characterize our memory using bright input pulses of many photons and detecting the pulses with a linear photodiode. We observe AFC echo efficiencies of just over 5% for $1/\Delta = 6$ μs and AFC spin-wave echo efficiencies of 1% for spin-wave storage time T_S of 18 μs. The reduction in efficiency is mostly due to imperfect control pulses. We estimate the transfer efficiency per control pulse to be roughly 0.5. By measuring the decay of the spin-wave echo as a function of T_S, we estimate the inhomogeneous spin linewidth to be 8 kHz. This measurement will be further detailed in a future publication. The 8-kHz linewidth is surprisingly low, a factor of 8 less than for the $^{153}Eu^{3+}$:Y_2SiO_5 (100 ppm) sample we previously used [33]. This results in a spin-wave memory time of $T_M = 50$ μs [defined as $\eta(T_M) = \eta(0) \exp(-1)$], the longest so far obtained in an AFC memory. By applying spin-refocusing techniques we can expect to increase it further, up to the spin coherence time of 15 ms [37].

IV. SINGLE-PHOTON-LEVEL PULSE STORAGE

We now turn to the main results of the this paper, storage of light pulses in the memory at the single-photon level. AFC spin-wave storage for weak coherent pulses with average photon numbers between $\bar{n} = 2.5 \pm 0.6$ and $\bar{n} = 11.2 \pm 0.6$ are shown in Fig. 2. The input pulse is 2 μs long, and the memory parameters are $1/\Delta = 6$ μs and $T_S = 21$ μs, leading to a total storage time of 27 μs. The duration and shape of the control pulses were optimized for the highest SNR; see discussion below. These measurements are performed, as all of the measurements shown in this paper, without the cryostat switched on to reduce the effect of vibrations on the comb structure [33].

There are two principal mechanisms which are responsible for the noise created by the bright control pulses. One is scattering of the laser light itself from optical surfaces. Another is emission from the atoms which have been excited by the pulses; this includes incoherent fluorescence, coherent free-induction-decay (FID) type emission, and an unexpected off-resonantly excited echo.

Spatial separation of the input and control modes is used to shield the single-photon-counting detector from scattered light, but this did not lead to sufficient suppression. A double-pass AOM [shown in Fig. 1(b)] is used as a detector gate in time, exploiting the temporal separation between the

FIG. 1. (Color online) (a) The atomic level scheme of the optical transition $^7F_0 \rightarrow {}^5D_0$ in $^{151}Eu^{3+}$:Y_2SiO_5. (b) A schematic of the experimental setup around the memory; the rest of the experiment has been suppressed for simplicity. The control and preparation beam is in single pass (wide labeled arrow). The input mode (thin dashed line) is in double pass, with the help of a Faraday rotator (FR) and a polarizing beam splitter (PBS). On return from the crystal the input mode passes through a Fabry-Perot (FP) cavity (bandwidth of 7.5 MHz). A classical detector (Sd) and 10 μW of horizontally polarized light (thin dotted line) are used to actively and intermittently stabilize the cavity to the frequency of the input mode. An acousto-optical modulator (AOM) in double pass acts as a detector gate.
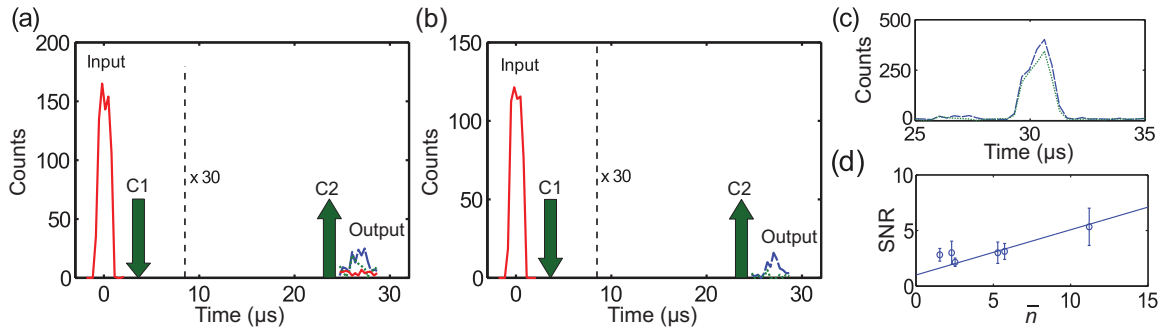
FIG. 2. (Color online) Storage of a weak coherent pulse with (a) $\bar{n} = 2.5 \pm 0.6$ and (b) $\bar{n} = 11.2 \pm 0.6$. The input mode recorded with no comb, the position of the control fields (C1 and C2), and finally a magnified ($\times 30$) signal of the AFC spin-wave echo (blue dashed curve), the associated noise without an input pulse (green dotted curve), and the detector dark counts (red curve) are shown. Note that the total measurement time differs between the data sets in panels (a) and (b). (c) The same echo data of panel (a) with the temporally separated off-resonant echo (OREO). (d) Signal-to-noise ratio (SNR) for different $\bar{n}$. Shown is also a fitted linear slope fixed to 1 at $\bar{n} = 0$ by definition.

control fields and the emitted spin-wave echo and providing a suppression of roughly 10^6. This proved sufficient to prevent detector blinding or significant afterpulsing.

However, the emission noise is also present in the temporal mode of the output mode. A diffraction grating and a Fabry Perot (FP) cavity are used to spectrally filter this noise. The FP cavity is necessary in particular to reduce noise originating from FID. Sharp spectral features about the control transition, by-products of the spectral tailoring required to prepare the AFC, cause the FID. We could reduce this noise by altering our preparation sequence to increase the transparency window around the control field transition. The frequency of this noise is close to that of the control field, a fact which we observe by changing the frequency at which we lock our FP cavity.

In addition to the fluorescence and FID noise, we also observed an unexpected noise source at the input frequency [see Fig. 2(c)], which occurs a time $1/\Delta$ after C2. These two observations suggest that the echo is produced by an off-resonant excitation of the comb by the control fields; we thus call this an off-resonant echo (OREO). The application of pulse C2 alone is enough to provoke this signal, but applying C1 strengthens it. We explain this by supposing that the off-resonant excitation of C1 is combined with transfer to the spin state. C2 then reads out the excitation in the same manner as it does the single-photon-level input pulse. Although the OREO is considerably larger than the AFC spin-wave echo which we are seeking to retrieve, the two echoes occur in temporally separated modes [see Figs. 2(a) and 2(c)]. We could reduce the impact of temporal mode leakage by carefully tuning the shape of the control fields, which is consistent with an off-resonant excitation mechanism. Note that since the FID and the OREO are coherent processes, the corresponding emission should only be strong in the control mode. Scattering inside the crystal, however, does introduce significant cross talk between the spatial modes.

The temporal shape of the remaining noise that we observe in Fig. 2(a) is indicative of FID noise. This gives us reason to believe that a more efficient filtering system would permit us to increase the power in the control fields, thus increasing their efficiency. The remaining noise, in this particular measurement, amounts to $(5.1 \pm 1.3) \times 10^{-3}$ photons per mode

emitted at the crystal. The SNR up to $\bar{n} = 11.2 \pm 0.6$ is shown in Fig. 2(d). These measurements were taken on a range of different days for the same experimental parameters. The SNR follows a linear dependence within the experimental errors; see the fitted linear slope in Fig. 2(d). Measurements carried out for higher average photon numbers (not shown) confirmed this behavior.

Averaging over all the measurements shown in Fig. 2(d), we obtain a global memory efficiency of $(3.8 \pm 1.5) \times 10^{-3}$ and an unconditional noise floor of $(7.1 \pm 2.3) \times 10^{-3}$. This weak pulse memory efficiency in the photon counting experiment was significantly lower than for the bright pulse storage (roughly 1%; see above). The optimization of the duration and shape of the control pulses led to a lower transfer efficiency. Furthermore, a photon-counting experiment requires time averaging; for example, the measurement for $\bar{n} = 2.5 \pm 0.6$ was taken over the course of 3 h. This challenges the stability of the experiment; in particular, laser fluctuations cause reduced quality combs, which negatively affect the AFC echo efficiency. We later discuss methods for solving these issues, which should lead to significantly higher SNR without increasing the noise floor.

V. COHERENCE MEASUREMENT

Finally we show the coherence of the AFC spin-wave echo. To do this we store a time-bin pulse in the memory where we vary the phase of one of the time bins. We then self-interfere the time-bin pulse using a temporal beam splitter and examine the interference curve. The visibility of the curve gives a measure of coherence preservation in the memory. For the measurement shown in this paper, the temporal beam splitter comes in the form of the control pulses. The scheme is pictorially shown in Fig. 3(a).

To store and analyze the time-bin pulse, we need clean temporal separation between the retrieved pulses and enough time to see the triple pulse structure shown in Fig. 3(c) after the final control field. To do this we extend the AFC time from 6 to 8 μs and reduce the pulse width of the input pulses and the entire pulse length of the control pulses. These measures further reduce the efficiency with which
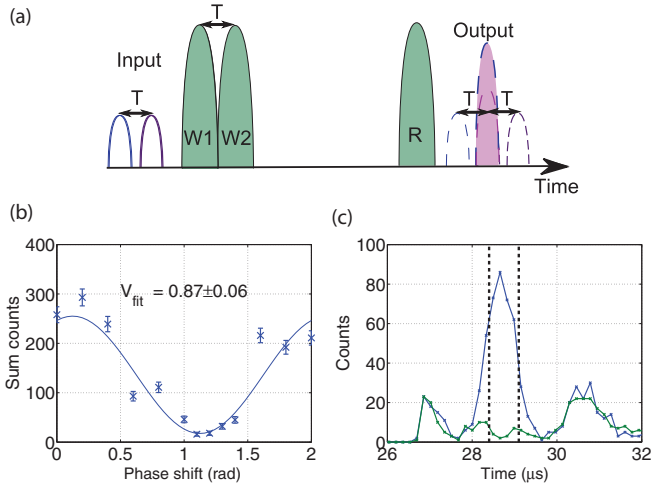
FIG. 3. (Color online) (a) The method used to measure the coherence of the AFC spin-wave echoes. The single-write operation of Figs. 2(a) and 2(b) (C1) is replaced by a double-write operation (W1, W2). If the temporal separation (T) of the input mode is equal to that of the double-write operation, the first echo of the second write operation and second echo of the first operation interfere. (b) The visibility curve for two pulses with $\bar{n} = 176 \pm 8$. (c) The signal of a constructive and destructive case. The thick dashed lines show the temporal window which was used to obtain the interference curve. The detector gate has cut some of the first echo and the OREO is not shown in this temporal slice.

we can store in the memory to $\eta_s = (6.3 \pm 0.1) \times 10^{-4}$ for each mode, including the reduction in storage efficiency due to the double-write operation. T_S was set to 21 μs in this experiment, yielding a total memory time of about 29 μs. A visibility curve for $\bar{n} = 176 \pm 8$ is shown in Fig. 3(b), where we measure $V = 0.87 \pm 0.06$. We suspect that laser phase noise contributes negatively to our visibility curve. A simple calculation shows that frequency noise with $\sigma_f = 25$ kHz reduces the baseline to $V = 0.95$. Together with the noise level this accounts for the visibility we measure. For $\bar{n} = 51 \pm 3$ we observe a further drop in visibility to $V = 0.71 \pm 0.1$. This is due to the increasingly important role of noise in determining the minimum of the visibility curve. We note that with higher storage efficiency, it should be possible to obtain high visibilities for lower photon numbers.

VI. DISCUSSION AND CONCLUSION

The unconditional noise floor achieved in our experiment should in principle allow us to store a single-photon-level optical pulse with high SNR. The limited SNR obtained at a few photons is entirely given by the low overall memory efficiency. This inefficiency is due to two major factors: (1) imperfect comb preparation and (2) insufficient control field transfer efficiency. (1) The optimal comb structure has square-shaped teeth [15,40] with negligible background absorption [19]. For our optical depth of 2.4, an AFC echo efficiency of 20% is theoretically possible [40]. Currently we are not able to create these high-quality combs due to the laser linewidth of 30 kHz. Recent high-resolution hole-burning experiments in Eu:Y$_2$SiO$_5$ support that this is possible [41].

To go beyond 20%, we would need to further increase the optical depth, using for instance an impedance-matched cavity configuration [24]. (2) The control field transfer efficiency can most easily be improved by using longer adiabatic transfer pulses [42], which in turn would require increased AFC echo time ($1/\Delta$). Increasing global efficiencies and achieving multimode capabilities thus primarily rely on using a stable laser with high spectral purity. It is important to note that the creation of a comb with higher spectral resolution and application of longer adiabatic control pulses is not likely to increase the noise floor, since neither optical depth nor control pulse power levels will need to be increased.

To conclude, we have demonstrated the first optical storage as a spin wave in a solid-state memory, in the regime of a few photons per input pulse. This was made possible by a strategy of extensive filtering and by carefully shaping the temporal envelope of the strong control pulses. The final unconditional noise floor of $(7.1 \pm 2.3) \times 10^{-3}$ is low enough to allow for quantum schemes using spin-wave storage and manipulation, such as the generation of quantum-correlated spin-wave and photonic excitations using a variant of the Duan-Lukin-Cirac-Zoller (DLCZ) [43] approach adapted to the solid-state [44–46]. Indeed, in Ref. [45], the relatively high unconditional noise floor (of around 1) prevented the observation of nonclassical correlations. Our results suggest that our filtering strategy could allow that, and similar experiments, to reach the nonclassical regime, due to an unconditional noise floor well below 1. These schemes will, in turn, allow for generation of entanglement between light and matter and entanglement of solid-state remote quantum memories, a basic building block for quantum repeaters.

APPENDIX: OREO PROPERTIES

We previously briefly described an unexpected noise source we encountered as we attempted to perform a complete AFC scheme with spin-wave storage at the single-photon level. The noise mechanism came in the form an echo which arrived at a time $1/\Delta$ after the application of the final control field (C2). We hypothesized that this echo was due to off-resonant excitation of the comb by the control fields and named the effect OREO (off-resonant echo). Here we present further data to support these conclusions.

We emphasize that the OREO is temporally separated from the AFC spin echo. Since it appears at time $1/\Delta$ after the last control fields, it will never directly interfere with any recalled optical pulse. Still, temporal mode leakage may well result in
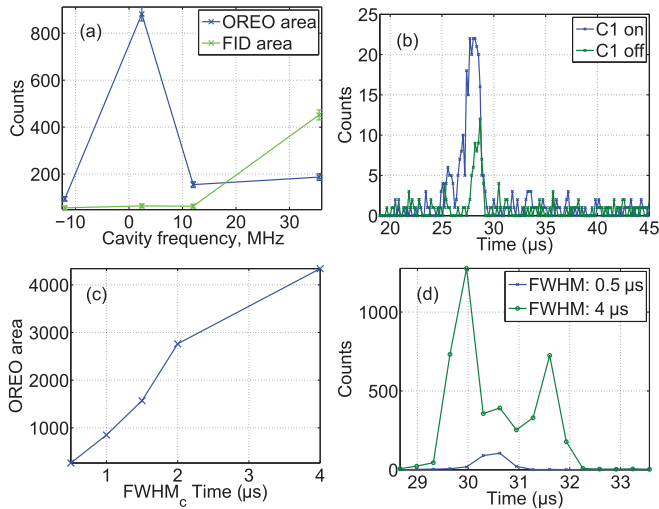
FIG. 4. (Color online) Experimental data, showing some of the main characteristics of the OREO. These include the emission frequency (a), the effect of the application of the first control field (C1) (b), and the relation between the magnitude of the OREO and the FWHM of the control field (c). Finally, in panel (d), we show the change in structure of the OREO, depending on the shape of the control fields used. See text for more details.
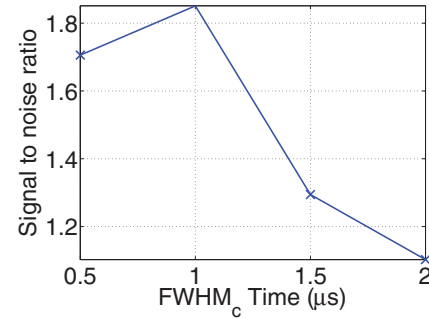

FIG. 5. (Color online) Experimental results showing the signal-to-noise (SNR) ratio as a function of the FWHM of the control pulse (see text for details). The average number of photons in the input pulse was 4.5 ± 0.5.

this effect being a potential problem. Therefore, understanding what causes this echo and how to reduce it is important for future experiments.

In Fig. 4(a) we show the measured OREO area [see Fig. 2(c) in the main text] where the filter cavity has been locked to different frequencies, slightly detuned with respect to the nominal frequency of the input-output pulses which we define to be 0. The highest OREO amplitude is measured at frequency 0. The extreme point at around $+35$ MHz corresponds to the frequency of the control pulses. This clearly illustrates that the OREO is an off-resonant excitation effect. In the same experiment we also looked at the amount of emission in a temporal window including both the temporal mode of the output and the FID signal appearing just after the detector gate was opened [see Figs. 1(a) and 1(b) for timing]. We see that the noise in this window increases significantly as the cavity frequency is tuned to the control field frequency at about $+35$ MHz. This supports our claim that this noise stems from free induction decay (FID) type emission caused by the control fields, where atoms close to the control pulse frequency are excited.

The effect of the first control field (C1) on the OREO is shown in Fig. 4(b). The second control field (C2) is present in both data sets shown in Fig. 4(b). One can see that the amount of OREO noise increases with the presence of both C1 and C2. To explain this we suppose that pulse C1 simultaneously excited the input frequency (off-resonantly) while transferring the excitation to the spin state. Such bichromatic excitation of spin coherences are actually used for spin-echo-type experiments [47]. In our case the excitation must be weak, since the bandwidth of pulse C1 is one order of magnitude smaller than the spin resonance frequency (35.4 MHz). The spin excitation is then read out with pulse C2. Note that both mechanisms, pulse C2 alone or pulses C1 and C2 combined, cause an echo a time $1/\Delta$ after pulse C2. One might think

that the bichromatic excitation by C1 cannot be completely instantaneous, but that the atoms spend a finite time as an optical coherence. This might explain why we observe a slight shift of the OREO emission toward earlier times when C1 is applied [compare curves in Fig. 4(b)].

We also observe that the shape of the control field has an effect on the magnitude of the OREO. We show this in Fig. 4(c). It should be pointed out that all pulses are defined within a fixed time slot, in this case of duration 2 μs. This is the time during which the AOM used in the control beam is turned on. Centered within this time slot we create a Gaussian pulse with a FWHM that is varied [x scale in Fig. 4(c)]. Note that the FWHM given here is that of the Gaussian pulse programed into the memory of the arbitrary function generator controlling the AOM. The actual FWHM will be slightly different due to the finite rise time of the AOM (300–400 ns) and the nonlinear response of the AOM system. For 0.5 μs FWHM the pulse is a smooth pulse, roughly Gaussian shaped, while for 4 μs FWHM the pulse closely resembles a square pulse. In Fig. 4(c) we observe a clear increase of the OREO noise as the pulse become more square, presumably due to stronger off-resonant excitation due to the sharp edges which give rise to high-frequency components. We also observe that the temporal shape of the OREO follows the shape of the control pulses. In Fig. 4(d) we show the OREO echo for the extreme cases of the control pulse FWHM; 0.5 μs (Gaussian) and 4 μs (square). We see that reducing the FWHM of the control fields yields a Gaussian-shaped OREO which is much smaller in magnitude.

From the studies of the OREO shown in Fig. 1, it is clear that to minimize it one should work with the smallest FWHM of around 0.5 μs, but it is also evident that the area of the pulse decreases as the FWHM is reduced, resulting in a strong decrease of the efficiency of the control pulses. It follows that one should measure the SNR of the output signal as a function of control pulse FWHM, in order to find the optimal value. This measurement is shown in Fig. 5. We see that for a FWHM of 1 μs, the optimum is reached. This particular control pulse was used for all experiments shown in Fig. 2 in the main text.

It should be emphasized that two additional parameters affect the SNR: (1) the bandwidth of the control pulse as a function of FWHM and (2) the FID-type emission noise. (1) As FWHM of the control pulses is increased, the bandwidth over which it is efficient is modified. Below we

present some numerical simulation of the transfer efficiency for parameters close to our experimental ones. (2) We have not discussed the FID noise, which is the dominant noise in the input-output temporal mode, for the optimum FWHM of 1 μs. The FID noise is much weaker than the OREO, making it difficult to make systematic studies of the FID noise [an exception being the study shown in Fig. 1(a)]. We simply want to point out that the optimum SNR found for a FWHM of 1 μs cannot be understood by considering only the OREO noise.

Finally we show some theoretical calculations of the control pulse efficiency and the off-resonant excitation probability, as a function of the FWHM of the control pulses. The calculations were done by numerically solving the standard two-level optical Bloch equations. The time slot of the control pulse was 2 μs, as in the experiment. The control-pulse Rabi frequency was set to 250 kHz, consistent with our experimental values. In order to calculate the global transfer efficiency, we take the Fourier transform of the input pulse of duration 2.2 μs and we multiply its power spectrum with the population transfer function of the control pulse. The global transfer efficiency is then obtained by integrating the resulting spectrum in frequency space. This takes into account the bandwidth mismatch between the input pulse and the control pulse. The off-resonant excitation probability is given by the population transfer function evaluated at 35.4 MHz and the frequency separation between the control and input-output frequencies.

In Fig. 6 we show the results of these simulations. They show the same behavior that we quantitatively predicted using simple arguments above. Between 0.5 and 4 μs FWHM there
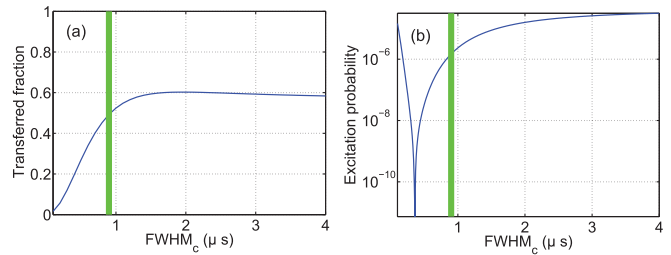

FIG. 6. (Color online) Simulations using a two-level Bloch equation simulator. Panel (a) shows the calculated transfer efficiency of a *single* control field. Panel (b) shows the off-resonant excitation probability, $+35.4$ MHz away from the carrier frequency. The horizontal scale shows the FWHM of a Gaussian pulse defined with the time slot of 2 μs. The thick (green online) line shows the optimal experimental FWHM.

is clearly a trade-off between control field efficiency (thus also global memory efficiency) and the amount of off-resonant excitation. The exact value of our experimental FWHM is shown by the thick line (green online). We again emphasize that the optimal SNR cannot be estimated solely with this model, since not all noise sources are included. It gives, however, theoretical support to our observations. We also emphasize that the maximum transfer efficiency of around 0.6 in Fig. 3(a) is not a fundamental limit. It is simply a result of the fact that in the simulations we have fixed the duration of the input pulse to 2.2 μs, the time slot of the control pulse to 2 μs, and the control field Rabi frequency to 250 kHz.

[1] N. Gisin, G. Ribordy, W. Tittel, and H. Zbinden, Rev. Mod. Phys. **74**, 145 (2002).

[2] D. Stucki, C. Barreiro, S. Fasel, J.-D. Gautier, O. Gay, N. Gisin, R. Thew, Y. Thoma, P. Trinkler, F. Vannel, and H. Zbinden, Opt. Express **17**, 13326 (2009).

[3] S. Wang, W. Chen, J.-F. Guo, Z.-Q. Yin, H.-W. Li, Z. Zhou, G.-C. Guo, and Z.-F. Han, Opt. Lett. **37**, 1008 (2012).

[4] J. F. Dynes, H. Takesue, Z. L. Yuan, A. W. Sharpe, K. Harada, T. Honjo, H. Kamada, O. Tadanaga, Y. Nishida, M. Asobe, and A. J. Shields, Opt. Express **17**, 11440 (2009).

[5] H.-J. Briegel, W. Dür, J. I. Cirac, and P. Zoller, Phys. Rev. Lett. **81**, 5932 (1998).

[6] C. Simon, H. de Riedmatten, M. Afzelius, N. Sangouard, H. Zbinden, and N. Gisin, Phys. Rev. Lett. **98**, 190503 (2007).

[7] N. Sangouard, C. Simon, H. de Riedmatten, and N. Gisin, Rev. Mod. Phys. **83**, 33 (2011).

[8] H. P. Specht, C. Nolleke, A. Reiserer, M. Uphoff, E. Figueroa, S. Ritter, and G. Rempe, Nature (London) **473**, 190 (2011).

[9] N. Piro, F. Rohde, C. Schuck, M. Almendros, J. Huwer, J. Ghosh, A. Haase, M. Hennrich, F. Dubin, and J. Eschner, Nat. Phys. **7**, 17 (2011).

[10] Y. O. Dudin, A. G. Radnaev, R. Zhao, J. Z. Blumoff, T. A. B. Kennedy, and A. Kuzmich, Phys. Rev. Lett. **105**, 260502 (2010).

[11] X.-H. Bao, A. Reingruber, P. Dietrich, J. Rui, A. Duck, T. Strassel, L. Li, N.-L. Liu, B. Zhao, and J.-W. Pan, Nat. Phys. **8**, 517 (2012).

[12] B. Julsgaard, J. Sherson, J. I. Cirac, J. Fiurášek, and E. S. Polzik, Nature (London) **432**, 482 (2004).

[13] K. F. Reim, P. Michelberger, K. C. Lee, J. Nunn, N. K. Langford, and I. A. Walmsley, Phys. Rev. Lett. **107**, 053603 (2011).

[14] M. Hosseini, G. Campbell, B. M. Sparkes, P. K. Lam, and B. C. Buchler, Nat. Phys. **7**, 794 (2011).

[15] C. Clausen, I. Usmani, F. Bussieres, N. Sangouard, M. Afzelius, H. de Riedmatten, and N. Gisin, Nature (London) **469**, 508 (2011).

[16] E. Saglamyurek, N. Sinclair, J. Jin, J. A. Slater, D. Oblak, F. Bussières, M. George, R. Ricken, W. Sohler, and W. Tittel, Nature (London) **469**, 512 (2011).

[17] C. Simon, M. Afzelius, J. Appel, A. Boyer de la Giroday, S. J. Dewhurst, N. Gisin, C. Y. Hu, F. Jelezko, S. Kröll, J. H. Müller, J. Nunn, E. S. Polzik, J. G. Rarity, H. De Riedmatten, W. Rosenfeld, A. J. Shields, N. Sköld, R. M. Stevenson, R. Thew, I. A. Walmsley, M. C. Weber, H. Weinfurter, J. Wrachtrup, and R. J. Young, Eur. Phys. J. D **58**, 1 (2010).

[18] J. J. Longdell, E. Fraval, M. J. Sellars, and N. B. Manson, Phys. Rev. Lett. **95**, 063601 (2005).

[19] H. de Riedmatten, M. Afzelius, M. U. Staudt, C. Simon, and N. Gisin, Nature (London) **456**, 773 (2008).

[20] E. Saglamyurek, N. Sinclair, J. Jin, J. A. Slater, D. Oblak, F. Bussières, M. George, R. Ricken, W. Sohler, and W. Tittel, Phys. Rev. Lett. **108**, 083602 (2012).

[21] C. Clausen, F. Bussières, M. Afzelius, and N. Gisin, Phys. Rev. Lett. **108**, 190503 (2012).

[22] I. Usmani, C. Clausen, F. Bussières, N. Sangouard, M. Afzelius, and N. Gisin, Nat. Photon. **6**, 234 (2012).

[23] M. P. Hedges, J. J. Longdell, Y. Li, and M. J. Sellars, Nature (London) **465**, 1052 (2010).

[24] M. Sabooni, Q. Li, S. Kröll, and L. Rippe, Phys. Rev. Lett. **110**, 133604 (2013).

[25] I. Usmani, M. Afzelius, H. de Riedmatten, and N. Gisin, Nat. Commun. **1**, 12 (2010).

[26] M. Bonarota, J.-L. L. Gouët, and T. Chanelière, New J. Phys. **13**, 013013 (2011).

[27] Z.-Q. Zhou, W.-B. Lin, M. Yang, C.-F. Li, and G.-C. Guo, Phys. Rev. Lett. **108**, 190505 (2012).

[28] M. Gündoğan, P. M. Ledingham, A. Almasi, M. Cristiani, and H. de Riedmatten, Phys. Rev. Lett. **108**, 190504 (2012).

[29] W. Tittel, M. Afzelius, T. Chanelière, R. Cone, S. Kröll, S. Moiseev, and M. Sellars, Laser Photon. Rev. **4**, 244 (2010).

[30] M. Afzelius, C. Simon, H. de Riedmatten, and N. Gisin, Phys. Rev. A **79**, 052329 (2009).

[31] J. Nunn, K. Reim, K. C. Lee, V. O. Lorenz, B. J. Sussman, I. A. Walmsley, and D. Jaksch, Phys. Rev. Lett. **101**, 260502 (2008).

[32] M. Afzelius, I. Usmani, A. Amari, B. Lauritzen, A. Walther, C. Simon, N. Sangouard, J. Minar, H. de Riedmatten, N. Gisin, and S. Kröll, Phys. Rev. Lett. **104**, 040503 (2010).

[33] N. Timoney, B. Lauritzen, I. Usmani, M. Afzelius, and N. Gisin, J. Phys. B **45**, 124001 (2012).

[34] M. Gündoğan, M. Mazzera, P. M. Ledingham, M. Cristiani, and H. de Riedmatten, New J. Phys. **15**, 045012 (2013).

[35] R. W. Equall, Y. Sun, R. L. Cone, and R. M. Macfarlane, Phys. Rev. Lett. **72**, 2179 (1994).

[36] F. Könz, Y. Sun, C. W. Thiel, R. L. Cone, R. W. Equall, R. L. Hutcheson, and R. M. Macfarlane, Phys. Rev. B **68**, 085109 (2003).

[37] A. L. Alexander, J. J. Longdell, and M. J. Sellars, J. Opt. Soc. Am. B **24**, 2479 (2007).

[38] J. J. Longdell, A. L. Alexander, and M. J. Sellars, Phys. Rev. B **74**, 195101 (2006).

[39] B. Lauritzen, N. Timoney, N. Gisin, M. Afzelius, H. de Riedmatten, Y. Sun, R. M. Macfarlane, and R. L. Cone, Phys. Rev. B **85**, 115111 (2012).

[40] M. Bonarota, J. Ruggiero, J.-L. Le Gouët, and T. Chanelière, Phys. Rev. A **81**, 033803 (2010).

[41] Q.-F. Chen, A. Troshyn, I. Ernsting, S. Kayser, S. Vasilyev, A. Nevsky, and S. Schiller, Phys. Rev. Lett. **107**, 223202 (2011).

[42] J. Minář, N. Sangouard, M. Afzelius, H. de Riedmatten, and N. Gisin, Phys. Rev. A **82**, 042309 (2010).

[43] L.-M. Duan, M. D. Lukin, J. I. Cirac, and P. Zoller, Nature (London) **414**, 413 (2001).

[44] P. M. Ledingham, W. R. Naylor, J. J. Longdell, S. E. Beavan, and M. J. Sellars, Phys. Rev. A **81**, 012301 (2010).

[45] S. E. Beavan, M. P. Hedges, and M. J. Sellars, Phys. Rev. Lett. **109**, 093603 (2012).

[46] P. Sekatski, N. Sangouard, N. Gisin, H. de Riedmatten, and M. Afzelius, Phys. Rev. A **83**, 053840 (2011).

[47] P. Hu, S. Geschwind, and T. M. Jedju, Phys. Rev. Lett. **37**, 1357 (1976).